Chapter 13

Colloidal Gold Nanoparticles Induce Changes in Cellular and Subcellular Morphology

Xiaowei Ma,[a,b,*] Raimo Hartmann,[a,*] Dorleta Jimenez de Aberasturi,[a,c] Fang Yang,[d,e] Stefaan J. H. Soenen,[f] Bella B. Manshian,[f] Jonas Franz,[g] Daniel Valdeperez,[a] Beatriz Pelaz,[a] Neus Feliu,[a,h,i] Norbert Hampp,[d,e] Christoph Riethmuller,[j] Henning Vieker,[k] Natalie Frese,[k] Armin Gölzhäuser,[k] Michael Simonich,[l] Robert L. Tanguay,[l] Xing-Jie Liang,[b] and Wolfgang J. Parak[a,c]

[a]*Fachbereich Physik, Philipps Universitat Marburg, 35037 Marburg, Germany*
[b]*Chinese Academy of Sciences (CAS) Key Laboratory for Biological Effects of Nanomaterials and Nanosafety, National Center for Nanoscience and Technology, Beijing 100190, China*
[c]*CIC biomaGUNE, 20009 San Sebastian, Spain*
[d]*Fachbereich Chemie, Philipps Universitat Marburg, 35037 Marburg, Germany*
[e]*Material Science Center, Philipps Universitat Marburg, 35037 Marburg, Germany*
[f]*Biomedical MRI Unit/MoSAIC, Catholic University of Leuven, 3000 Leuven, Belgium*
[g]*nAnostic Institute, Center for Nanotechnology, University of Münster, 48149 Münster, Germany*
[h]*Department of Laboratory Medicine (LABMED), Karolinska Institutet, SE-17177 Stockholm, Sweden*

Reprinted with permission from *ACS Nano*, **11**, 2017.

*These authors contributed equally to this work.

Bio-Nano Interfaces: Perspectives, Properties, and Applications
Edited by Wolfgang J. Parak

ISBN 978-981-4877-83-1 (Hardcover), 978-1-003-30649-8 (eBook)
www.jennystanford.com

[i]*Medcom Advance S.A., 08840 Barcelona, Spain*
[j]*Serend-ip GmbH, Center for Nanotechnology, 48149 Münster, Germany*
[k]*Fakultät für Physik, Universität Bielefeld,, 33615 Bielefeld, Germany*
[l]*Sinnhuber Aquatic Research Laboratory (SARL), Oregon State University, Corvallis, Oregon 97331, United States*
liangxj@nanoctr.cn, wolfgang.parak@physik.uni-marburg.de.

Exposure of cells to colloidal nanoparticles (NPs) can have concentration-dependent harmful effects. Mostly, such effects are monitored with biochemical assays or probes from molecular biology, i.e., viability assays, gene expression profiles, etc., neglecting that the presence of NPs can also drastically affect cellular morphology. In the case of polymer-coated Au NPs, we demonstrate that upon NP internalization, cells undergo lysosomal swelling, alterations in mitochondrial morphology, disturbances in actin and tubulin cytoskeleton and associated signaling, and reduction of focal adhesion contact area and number of filopodia. Appropriate imaging and data treatment techniques allow for quantitative analyses of these concentration-dependent changes. Abnormalities in morphology occur at similar (or even lower) NP concentrations as the onset of reduced cellular viability. Cellular morphology is thus an important quantitative indicator to verify harmful effects of NPs to cells, without requiring biochemical assays, but relying on appropriate staining and imaging techniques.

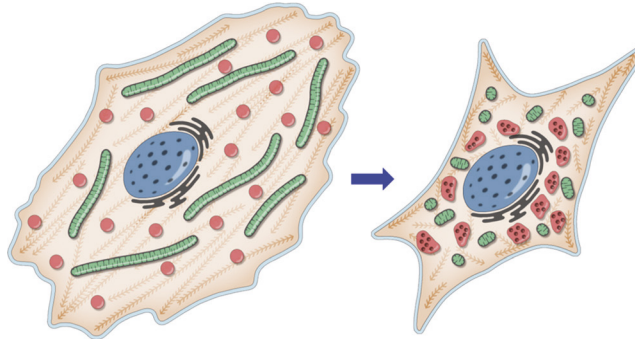

Colloidal nanoparticles (NPs) are incorporated by living cells, regardless of whether this is intended for certain delivery applications

(i.e., tumor targeting) or unintended, e.g., due to leakage of NPs into the environment (i.e., air, water pollution) [1]. Once in contact with cells, the typical uptake scenario involves endocytosis [2–4]. Proteins adsorbed to the surface of the NPs hereby play a major role [5, 6]. Interaction of NPs with cells has been demonstrated to trigger dose-dependent effects in cells (which obviously strongly depend on the nature of NPs and on the type of cells), which can ultimately lead to cell death. Details about the uptake mechanisms of NPs by cells, as well as the molecular signaling cascades which are being triggered [7], in particular involving molecular mechanisms for toxic effects, are well described in the literature [8–10]. Most of these studies aim at understanding the interaction of NPs with cells at a molecular level. However, effects of the NPs on cells are also manifested at the level of cell morphology. Due to high-throughput microscopy and high content screening of the acquired data, the assessment of morphological parameters is becoming more and more feasible allowing for multiparametric response and cytotoxicity studies to be carried out [11–13].

In multiple studies the disruption of organelles and other subcellular structures caused by NPs have been reported. Gold NPs for example (as well as other NPs) have been described to have a profound effect on several intracellular organelles/structures and functions associated with morphological changes. First, this applies to mitochondria. Mitochondria are one of the most important organelles in cells. Damage/disruption of mitochondria can result in a wide range of diseases and disorders. It has been reported that the decrease of mitochondrial activity reflects acute cytotoxicity of colloidal NPs [14]. Many studies have found that exposure of cells to Au NPs was accompanied by an increased level of reactive oxygen species (ROS), which is associated with malfunctioned mitochondria. Pan *et al.* observed that Au NPs of an average diameter of 1.4 nm induce cytotoxicity by oxidative stress, which is indicated by endogenous ROS production, compromised mitochondrial potential, integrity, and mitochondrial substrate reduction [15]. Interestingly, Chompoosor *et al.* reported that 2 nm Au NPs with different hydrophobic alkyl tails could generate significant amounts of ROS at concentrations that do not even affect mitochondrial activity [16]. Mkandawire *et al.* used Au NPs conjugated with a mitochondrial localization signal to target mitochondria for activation of intrinsic apoptotic pathways.

It was found that the mitochondrial outer membrane was partially ruptured, and cell death was triggered [17]. Wang *et al.* speculated that the selective targeting and damaging effects of Au nanorods to the mitochondria of cancer cells could be used in tumor therapy, while normal cells maintain intact mitochondria [18]. For NPs of other materials and sizes, even mitochondrial permeabilization and fragmentation were observed [19]. Second, effects on lysosomes have been reported. Most NPs will eventually be accumulated inside acidic organelles after following their endocytic pathway. Being the major degradative compartment of eukaryotic cells, the lysosome is a high capacity organelle responsible for macro-molecular homeostasis. Previous work has shown that large amounts of Au NPs aggregated in the lysosomes can lead to lysosome alkalinization. This is associated with the impairment of vacuolar V-ATPases, which regulate lysosome acidification. Consequently, the lysosome-based degradative autophagy pathway is affected, which leads to a disruption of cellular homeostasis [20]. Swelling of lysosomes upon NP enrichment has also been reported [14, 21, 22]. Recently, Gunduz and co-workers reported that rapid intracellular accumulation of Au NPs resulted in elevated endoplasmic reticulum stress. Above a certain threshold, inhibition of macropinocytosis ceased further uptake of Au NPs, and endoplasmic reticulum stress was reduced [23]. Third, NPs have been shown to interfere with the cellular cytoskeleton [24]. The cytoskeleton is responsible for anchoring organelles, maintaining cell morphology, and intercellular connections. Previous findings by Pernodet *et al.* indicate that the diameter, the stretching state, and the density of actin filaments in human dermal fibroblasts were affected in a concentration-dependent manner upon treatment with Au NPs. These effects might cause major changes in cell shape, cell spreading, cell adhesion, and cell growth [25–27]. The same group also found that different sized Au NPs (13 or 45 nm) can induce cytoskeletal filament disruption to a different extent, without changing actin or beta-tubulin protein levels [28]. A further study by Yang *et al.* showed that the actin F-fibers were disrupted to various extents depending on the aggregation state of Au NPs. The authors reported varying decrease in F-actin fiber intensity and thickness and the appearance of actin dots. The lack of actin-fiber formation and the appearance of actin dots rather than long fibers were correlated with the presence of Au NPs in the cytosol which were thought to cause depolymerization

of actin [29]. Furthermore, the morphology of cell junctions may be subject to changes [30, 31] following NP exposure. The intracellular disruption of the cytoskeletal network caused by Au NPs has been found to be associated with the disruption of cell–cell adhesion. It was found that exposure to highly concentrated Au NPs will significantly reduce the area of focal adhesion complexes (FACs), which leads to an increase in the amount of free vinculin, a major structural component of FACs [12]. Lin *et al.* also found different sized Au NPs could cause loosening of the intercellular tight junctions that are joining individual cells [32]. Moreover, the phenotypic changes of lung fibroblasts might be affected by cocultured small airway epithelial cells which were treated with Au NPs. Morphological changes observed include an increase in vinculin adhesion and altered F-actin stress fiber arrangement [33]. Finally, NP impact on the cytoskeleton may influence cellular migration. Rafailovich's group found that the presence of Au NPs in human adipose-derived stromal cells could result in a concentration-dependent increase in population doubling times, a decrease in cell motility, and cell-mediated collagen contraction [34]. Considering that cell migration plays a crucial role in tumor growth and metastasis, therefore, NPs that can impede the mobility of tumor cells are of great interest in preclinical research. In summary, there is clear evidence that the uptake of Au NPs by cells has a (concentration-dependent) effect on their morphology.

In the present work, we provide a comprehensive study on how in vitro uptake of Au NPs affects cellular morphology and intracellular organelles/structures. Thus, the focus of this work is not on signal pathways, but rather on morphological changes, in particular on using a set of different techniques and to compare these data. Concerning methodologies, we attempted to use as many different techniques as possible to probe cell morphology, most of them based on imaging and structural analysis of different cellular compartments. Concerning the NPs, polymer-coated, anionic Au NPs (Au-PMA* NPs) with a fluorescent label were chosen for this study [12, 35–37]. These NPs have been fully characterized for their colloidal properties and interaction with cells within the last 10 years. They are colloidally stable with a narrow size distribution (4.8 ± 0.7 nm core diameter) [38, 39]. These NPs are incorporated by cells *via* endocytic pathways and accumulated inside acidic intracellular vesicles, in particular lysosomes [40–42]. In contrast to other NPs such as cadmium

selenide (CdSe) or silver (Ag) NPs, the Au NPs are not composed of an intrinsically toxic material, yet several concentration-dependent cytotoxic responses such as production of ROS have been described in vitro [12, 43]. Reported IC_{50} concentration values for Au NPs of similar size distribution vary between a few hundred nM [12, 44] and a few μM or even mM [45, 46] depending on surface coating, the cell types used, and incubation conditions. The NPs used in the present study are bigger than the ultrasmall clusters of 1.3 nm core size Au NPs for which size-specific effects have been reported [15]. In the case of the here used ca. 4.8 nm core diameter NPs toxic effects do not only originate from their surface coating but are also due to the Au core [43], which possesses some catalytic activity. As control, the same Au NP cores, but with different surface coating (i.e., PMA without a fluorescence label, mercaptoundecanoic acid (Au-MUA NPs [47]), and polyethylene glycol (Au-PEG NPs [47, 48]) were used. In addition, Au^{3+} (as obtained from hydrogen tetrachloroaurate (III) hydrate, $HAuCl_4 \cdot xH_2O$), and Cd^{2+} (as obtained from $CdCl_2$) was used as reference [49] as well as empty PMA polymer micelles.

For this study two well-established and commonly used mammalian cell lines were used. These were the human umbilical vein endothelial cells (HUVECs) and the human cervical cancer cell line (HeLa). HeLa cells are human cervical carcinoma cells that have been widely applied as a model system for cancerous cells in bionano interaction studies, including cytotoxicity and cellular up take studies of various types of NPs, including Au NPs [50, 51]. HUVECs are primary human umbilical vein endothelial cells and were obtained as pooled aliquots from different samples to minimize heterogeneity due to differences between donors. HUVECs are a widely used model of primary cell cultures and can be further used to represent an in vitro alternative to endothelial cells lining the blood vessels, in particular in newly growing vessels such as those formed during angiogenesis in tumor formation [52]. The cells were used from passage 5–10 after isolation for any experiments and have also been frequently used for nanobio interaction studies. Both cell types also have a high biomedical relevance, where HUVEC cells are often labeled with NPs to enable non-invasive monitoring of cell transplantation efficacy [53]. HeLa cells represent a model for cancer cells, as the main biomedical application of NPs lies in the field of oncological research [54]. The combination of a cancer cell line and a primary cell type enabled us to further compare whether

the observed mechanisms are specific for either one of the cell types or whether this is of a more general nature.

13.1 Results and Discussion

13.1.1 Au-PMA* NP Location and Internalization Rate

Cellular internalization of Au NPs by HeLa and HUVEC was investigated in terms of fluorescence microscopy and flow cytometry. As expected, the Au NPs were internalized by both HeLa cells and HUVECs. While we did not make attempts to unravel the detailed uptake pathways (i.e., by blocking of certain pathways by specific inhibitors or by colocalization experiments with objects of known pathways of internalization), it is known from previous experiments with NPs of similar surface chemistry that the Au NPs are endocytosed by cells [12] Experiments have shown contribution of macropinocytosis (see for example the formation of macropinocytic cups upon NP internalization, *cf.* TEM images in the Supporting Information, Section IV) as well as caveolin-mediated endocytosis [41]. Presence of the Au NPs in the lysosomes after cellular internalization was proven by colocalization of the fluorescence-labeled NPs with green fluorescent protein (GFP)-labeled lysosomal-associated protein 1 (LAMP1), employing confocal laser scanning microscopy [55]. LAMP1 was expressed in HUVEC and HeLa cells as a marker for lysosomal membranes. Quantification of internalized NPs demonstrates that for HUVECs (in 2% serum supplemented medium) the uptake rate of Au NPs was higher and that transport of the Au NPs into the lysosomes (c_{NP} = 25, 50, 100 nM NP concentration) was faster as compared to HeLa cells (in 10% serum supplemented medium). In case of HUVECs, saturation of cells with NPs was already seen after <5 h, whereas in HeLa cells the amount of internalized NPs still increased after 15 h (see Fig. 13.1 and Supporting Information, Section XI). In the case of HUVECs, incubation with the double amount of NPs (from 25 to 50 nM) resulted also in more or less the double amount of internalized NPs. A similar trend was observed in the case of HeLa cells. However, even within 24 h of exposure, HeLa cells were not saturated with Au NPs at the used concentrations. Uptake of the Au NPs by HeLa cells thus follows a slower kinetics compared to the HUVECs. We have also

noted that differences in the amount of serum in the culture medium may play a role in the NP uptake, as serum in general reduces NP uptake [39]. Our results highlight the effects of the serum on the uptake of NPs to cells.

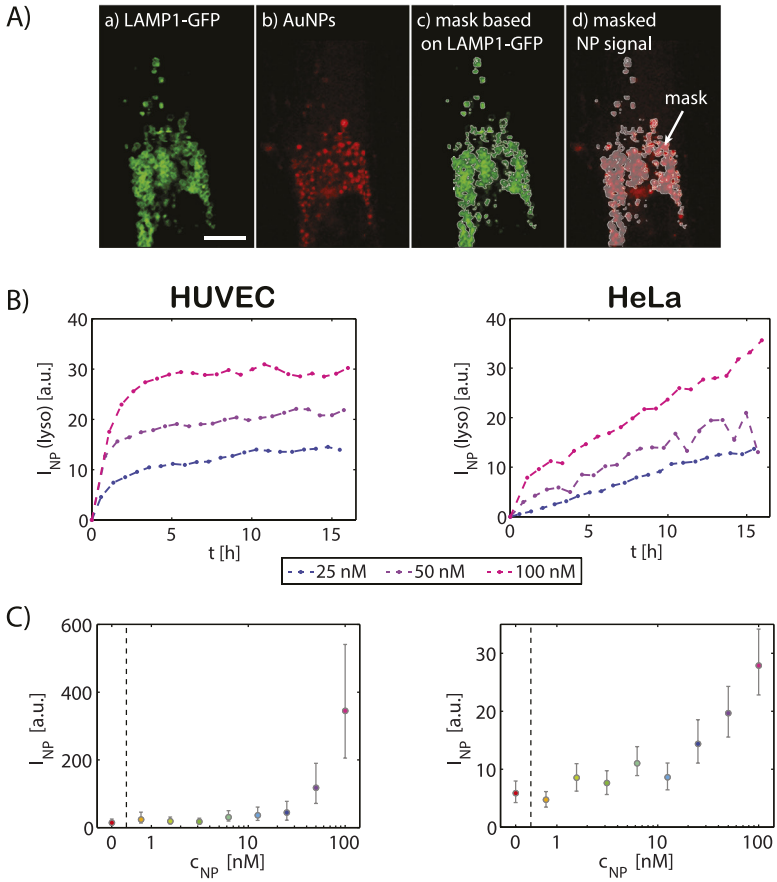

Figure 13.1 Uptake of Au NPs by HUVEC and HeLa cells. (A) Confocal micrographs of HUVEC exposed to Au-PMA* NPs for 16 h at c_{NP} = 50 nM. (a) The signal of stained lysosomes is used to create a mask. (b) Channel of fluorescence-labeled NPs. (c) Mask based on LAMP1-GFP signal. (d) Mean intensity I_{NP}(lyso) of NPs inside the lysosomal mask. The scale bar corresponds to 10 μm. (B) Mean NP-intensity I_{NP}(lyso) measured inside lysosomal structures at different Au-PMA* NP concentrations c_{NP} = 25, 50, and 100 nM. (C) Integrated fluorescence intensity of internalized Au-PMA* NPs per cell (I_{NP}). The results are presented as normalized probability distributions (first row) and median ± lower/upper quartile for 500–1000 cells/condition.

Table 13.1 Summary of the experimental results in which cellular reaction to exposure to Au-PMA* NPs was probed[a]

				Trend		$C_{NP,50}$ range [nM]	
Feature	**Parameter**	**Variable**	**Derived from**	***HUVEC***	***HeLa***	***HUVEC***	***HeLa***
NP uptake	Integrated intensity	I_{NP}	NP fluorescence	+++	+		
Viability	Viability	V_{res}	Resazurin ("Marburg")	–	–	3.5–**11**–33	
		V_{AB}	Resazurin ("Leuven")	–	0	55–**65**–77	
		V_{MTT}	MTT	–	–	2.7–**8.4**–27	
	Dead/live	D	live/Dead stain	+	+	30+	80+
	Proliferation rate	P	DNA synthesis	–	–	0.49–**0.54**–0.59	0.073–**0.12**–0.20
	ROS	R	Pyocyanin/N–acetyl–L–cysteine	++	+	10+	10+
Cell morphology	Area	A_{cell}	CellMask blue	–	–	18–**26**–37	39–**49**–61
			Actin (phalloidin)	–	–	2+	10+
		A_{nuclei}	DAPI	0	0		
	Form factor	F_{cell}	Actin (phalloidin)	0	–		8+
Lysosomes	Area	A_{lygo}	LAMP1 (Ab)	+++	o	5+	
	Fraction of cell area	A_{lyso}/A_{cell}	LAMP1 (Ab) /actin (phalloidin)	++	++	30+	10+
	Intensity	I_{lyso}	LAMP1 (Ab)	0	+		10+

(*Continued*)

Table 13.1 (*Continued*)

Feature	Parameter	Variable	Derived from	Trend		$C_{NP,50}$ range [nM]	
				HUVEC	***HeLa***	***HUVEC***	***HeLa***
Mitochondria†	Form factor	F_{mito}	CellLight – mitochondria	+++	+++	0.083–**0.45**–2.5	0.082–**0.34**–1.4
	Zernike 0th order	Z^0_{mito}		+++	+++	0.13–**0.29**–0.64	0.080–**0.20**–0.51
Cytoskeleton	Filopodia: Area	A_{vinc}	Vinculin (Ab)	–	–	50+	50+
		A_{filo}		–	0/–	2+	25+
	Filopodia: Number	N_{filo}	AFM	–	–	2+	50+
	Filopodia: Volume	V_{filo}		–	–	2+	25+
	Filopodia: Height	h_{filo}		0	0		
	Actin: Texture contrast	$T_{act,cont}$	Actin (phalloidin)	+	–	5+	1.7–**3.3**–6.3
	Actin: Texture correlation	$T_{act.corr}$		+	–	5+	5+
	Tubulin: Texture contrast	$T_{tub,cont}$	Tubulin (Ab)	+	/	50+	/
	Tubulin: Texture correlation	$T_{tub,corr}$		–	/	10+	/

Feature	Parameter	Variable	Derived from	Trend		$C_{NP,50}$ range [nM]	
				HUVEC	*HeLa*	*HUVEC*	*HeLa*
	Gene expression	CALDl	RT-PCR array	+	+	12+	25+
		CCNA1		+	+	50+	25+
		CYFIP2		++	++	25+	25+
		IQGAP2		+	++	50+	12+
		MAPK13		+++	+	25+	50+
		MAPT		++	0	25+	
		PPP1R12A		+	0	50+	
		PPP1R12B		+	++	50+	12+
		TIAM1		+	++	50+	12+
		VASP		0	+		(50+)

[a]Reactions are shown in the trend column. $c_{NP,50}$ describes the NP concentration at which half of the maximum effect was obtained. If a sigmoidal fit could be applied to the data, then the uncertainty is given in addition. The full data sets corresponding to this table are shown in the Supporting Information. Ab = antibody.

13.1.2 Effect of Au-PMA* NPs on Cell Viability, Proliferation, and Other Indicators

It is well-known that even inert Au NPs can cause cytotoxic effects on cells at elevated exposure concentrations and times. In order to investigate a useful range of concentrations, we took into account two considerations. First, in case of biological in vitro labeling experiments, NP concentrations are typically chosen in the range of a few to a few tens of nM, in order to provide sufficient effect. Second, as according to Paracelsus, everything at high enough concentration is toxic, we performed in vivo toxicity experiments with zebra fish embryos. Exposure of zebrafish embryos to NP concentrations up to 700 nM was not significantly associated with mortality or any morphological abnormality, which demonstrates the relatively low toxic profile of the here used Au NPs (see the Supporting Information, Section XV for the data). Guided by these two considerations, we decided to investigate NP concentrations in the range from 0.1 to 100 nM, which covers the range of typical in vitro applications, but does not cause any acute abnormality in vivo. Using this range of concentrations, we performed several standard biochemical assays to investigate the concentration-dependent effect of Au NPs on HUVECs and HeLa cells (see the Supporting Information, Section IX for raw data). As exposure time for all following experiments, we chose 24 h. In a first set of assays, effects on cellular enzymatic activity were probed: (i) oxidation of resazurin (Alamar blue) by cellular dehydrogenases (Resazurin assay/Alamar blue assay) likely inside mitochondria; (ii) reduction of 3-(4,5-dimethylthiazol-2-yl)-2,5-diphenyltetra-zolium bromide (MTT) by oxidoreductases (MTT assay); and (iii) conversion of cell permeable calcein acetoxymethyl (AM) by esterases (first part of a commercial Live/Dead assay). In order to probe for interlaboratory variation, the resazurin assay was carried out as well in the Marburg as in the Leuven laboratory, according to the local standard protocols. In HUVECs, the resazurin ("Marburg") as well as the MTT assays showed reduction of cell viability at around $c_{NP,50} \approx 10$ nM (all raw data can be found in the Supporting Information, and a summary of all effects is shown in Table 13.1), whereas in case of the resazurin ("Leuven") and

the "Live" assay, these effects were detected at slightly higher concentrations of NPs. Comparison of the results for the resazurin assay as carried out with the local protocols of different laboratories demonstrates that absolute values have to be interpreted with care, and variation between different laboratories may occur. In the case of HeLa cells, the effect of the Au NPs on cell viability was much lower, and exposure with NPs up to concentrations of 100 nM could in most assays not reduce viability to its half. Still, also in HeLa cells, concentration-dependent reduction in cell viability was observed. In a second assay format, cellular proliferation was probed in terms of measuring DNA synthesis. For both cell lines, inhibition of proliferation was already caused by NP concentrations well below 1 nM. Cellular proliferation thus is at least sensitive to 1 order of magnitude lower NP concentrations than cellular viability. In a third assay, we probed for direct damage: In the "Live/Dead" assay a cell-impermeable ethidium homodimer only stains cellular nuclei in case their membrane is damaged in the form of perforation. Altogether the $c_{NP,50}$ values obtained from the Live/Dead assay were in the range of a few tens of nM. Images of the outer cell membrane with helium ion microscopy also show disruption of the cellular plasma membrane at high NP concentrations (see the Supporting Information, Section VI for the data). In a fourth assay type, we probed for the generation of ROS, which are typically associated with cytotoxic effects, using CellROX Green as the probe. For both cell types, we found $c_{NP,50}$ values of around 10 nM. First, these data (*cf.* Table 13.1) show that significant reduction in cellular proliferation starts already at least at 1 order of magnitude lower Au NP concentrations, which corresponds to the concentration at which cellular viability is affected. Second, viability of HeLa cells is less influenced by the exposure to Au NPs than HUVECs. Onset of oxidative stress (production of ROS) starts at similar NP concentrations as required to reduce cell viability (see Fig. 13.2). More dramatic effects such as permeation of nuclear membranes occur at even higher NP concentrations. Summing up, these data indicate that first toxic effects of Au NPs can be already noted at NP concentrations well below 1 nM (proliferation), whereas typical onset of drastic reduction in cell viability requires exposure concentrations in the order of 10 nM.

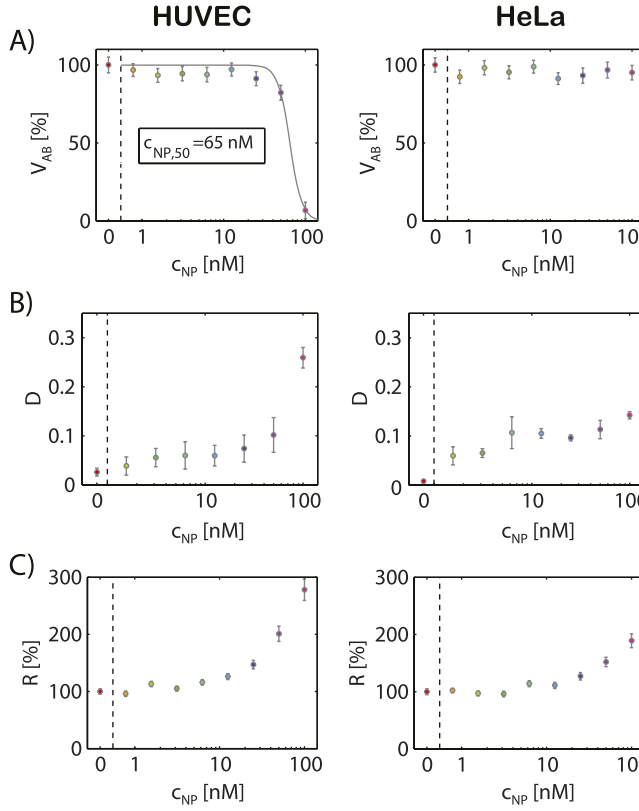

Figure 13.2 Effect of Au-PMA* NPs on cell viability and oxidative stress. (A) Cell viability V_{AB} of HUVECs and HeLa cells exposed to different concentrations c_{NP} of Au-PMA* NPs, as determined with the Alamar blue test. (B) Rate of dead *versus* live cells D upon exposure to Au-PMA* NPs to cells, as derived from a fluorescence cell staining specific for live and dead cells, respectively. (C) ROS levels R of cells exposed to Au-PMA* NPs. Results are presented as mean value ± SD for n = 3–4 independent measurements.

13.1.3 Lysosomal Swelling Caused by Endocytosed Au-PMA* NPs

Staining of the lysosomes (yellow stain in the corresponding images in Figs 13.3 and 13.4, see the Supporting Information, Section XI for the raw data) as well as of the cytoskeleton allows for relating the average sectional area of lysosomes A_{lyso} to the cell cross-section area A_{cell} in a defined intracellular plane, *cf.* Fig. 13.4A. Thereby, a useful

measure, the fraction of cell area which is occupied by lysosomes A_{lyso}/A_{cell} can be derived. The results clearly indicate that lysosomes start to swell, i.e., increase their size, upon exposure of cells to NPs, whereby the effect was higher for HUVECs than for HeLa cells (*cf.* Fig. 13.4C and Table 13.1). Just looking at the size of lysosomes already allows for pre-estimating whether NPs are present. The $c_{NP,50}$ values, e.g., the required NP concentration at which half of the effect is observed, are on the order of 10 nM. In summary, exposure of cells to NPs causes swelling of lysosomes, thus leading to an increased fraction of intracellular space which is occupied by lysosomes.

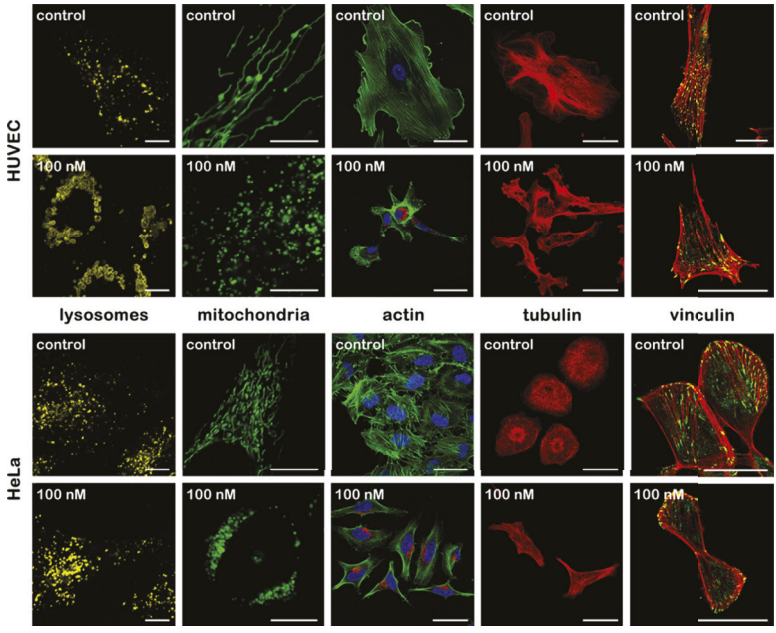

Figure 13.3 Morphological changes of different cellular structures without and after c_{NP} = 100 nM Au-PMA* NP treatment in HUVECs and HeLa cells. All scale bars correspond to 50 µm, except for lysosomes and mitochondria (10 µm). Lysosomes were stained with antilysosomal-associated protein 1 (LAMP1) antibodies (shown here in yellow false colors). Mitochondria were stained by expressing green fluorescent protein GFP-labeled E1 alpha pyruvate dehydrogenase in the cells (shown in green). Actin fibers were stained by phalloidin (shown in green), nuclei stained with DAPI (shown in blue), together with the red fluorescence of incorporated NPs. Tubulin was stained using an anti-alpha tubulin antibody (shown here in red). Vinculin was stained with an antivinculin mouse monoclonal antibody (shown in green), together with actin staining with phalloidin (shown in red).

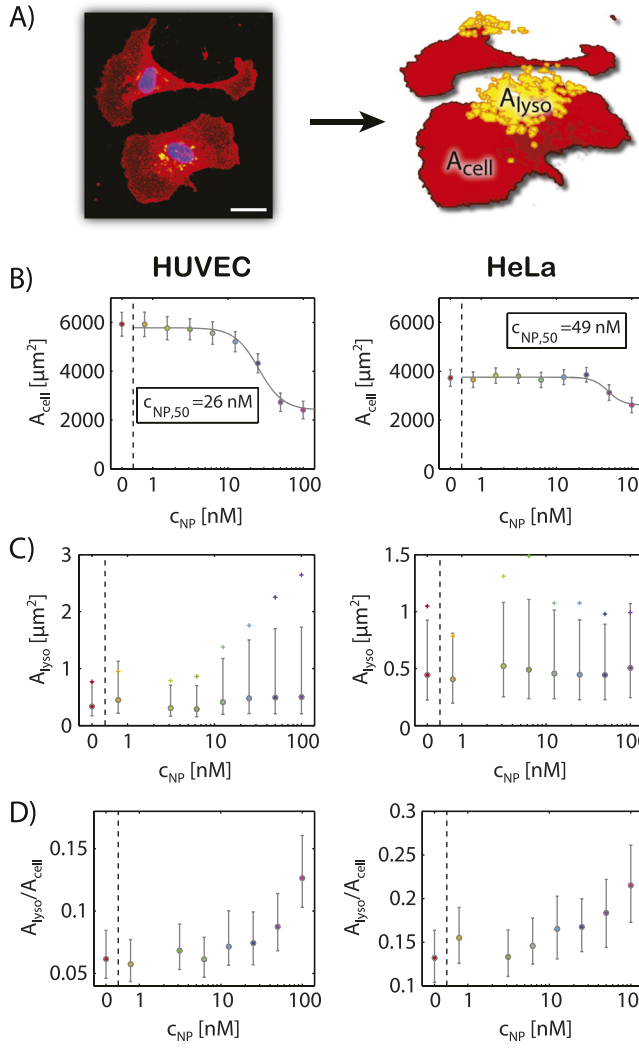

Figure 13.4 Effects of Au-PMA NPs on the lysosome. (A) The lysosomal fraction is calculated by dividing the area occupied by lysosomes (A_{lyso}) by the area of the whole cell (A_{cell}). Left image: blue: nuclei, red: plasma membrane, scale bar: 20 µm. (B) Mean cross section area per cell A_{cell} of HUVECs (left) and HeLa cells (right), which had been incorporated for 24 h with Au-PMA* NPs at different concentrations c_{NP}. Error bars indicate ± SD for 3 independent sets of over 2000 cells evaluated per condition. (C) Size of individual lysosomes after cells had been exposed to Au-PMA* NPs at different concentrations c_{NP}. (D) Fraction of area occupied by lysosomes related to the whole cell cross section area A_{lyso}/A_{cell}. The results are presented as median (o) ± lower/upper quartile for 1800–4000 lysosomes/condition. The mean values are represented as crosses (+).

13.1.4 Loss of Mitochondrial Structure Caused by Au-PMA NPs (Without Label)

Staining of the mitochondria (green stain in the corresponding image in Fig. 13.3, see the Supporting Information, Section XII for the raw data) allowed for observing changes in the morphology of the mitochondria upon cellular exposure to Au NPs. Data show that upon presence of NPs, there is a significant shape change from more thread-like elongated to smaller spherical structures. This can be quantified by calculating the form factor F_{mito} and the Zernike moment of zeroth order Z^0_{mito}, *cf.* Table 13.1, Fig. 13.5. Both measures describe the transition from an indefinitely extended object (F, Z_0 = 0) to a spherical object (F, Z_0 = 1) [56]. The results clearly indicate dramatic changes in mitochondrial morphology upon exposure to NPs. As mitochondria are the "power plant" of cells, thus energy availability might be affected. For both investigated cell types, the $c_{\mathrm{NP,50}}$ values were between 0.1 and 1 nM and, therefore, well below NP concentrations in which reduction of cellular viability was detected. Thus, reduction in cellular viability might be interpreted as a consequence of mitochondrial impairment.

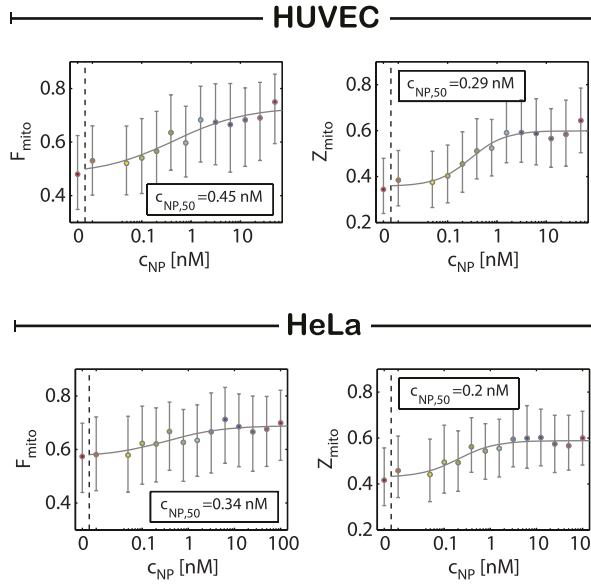

Figure 13.5 Geometrical features (form factors F_{mito} and Zernike coefficients of 0$^{\mathrm{th}}$ order Z_{mito}) of mitochondria upon exposure to Au-PMA NPs (without fluorescence label) to cells. The results are presented as median ± lower/upper quartile for 1700–5000 mitochondria/condition).

13.1.5 Distortion of the Cytoskeleton Caused by Au-PMA* NPs

Staining of several components of the cell cytoskeleton was performed, *cf.* Fig. 13.3 (the raw data are presented in the Supporting Information, Section XIII). Actin was stained with fluorescence-labeled phalloidin, while specific antibodies were used for tubulin and vinculin staining procedures. Even by microscopic inspection with the naked eye, striking effects of the NPs on the morphology of the cells were visible. Presence of NPs strongly reduced the cellular cross-section area A_{cell}. In the case of HeLa cells, NP exposure induced a more elongated, stretched cell shape, manifested by a reduction in the form factor F_{cell}, *cf.* Fig. 13.6A and Table 13.1. Actin fibers were directly affected by exposure to the NPs. In the case of HUVECs, the elongated actin fiber bundles shortened and rounded up. In the case of HeLa cells, the actin fibers appeared smoother, indicated by a decreasing texture contrast $T_{\mathrm{act,cont}}$ [57]. For tubulin, an increase in texture contrast $T_{\mathrm{tub,cont}}$ and decrease in texture correlation $T_{\mathrm{tub,corr}}$ were observed in case of HUVECs, see Fig. 13.6B. Under high NP doses, tubulin fibers were arranged less compactly and became thinner and longer. Visual inspection with the naked eye however leads to the conclusion that the tubulin network is less affected than the actin network by the presence of NPs. The cytoskeleton stabilizes cells in a dynamic way, based on continuous polymerization and depolymerization of fibers. For this reason control experiments without involving cells were performed, in which reduction of actin and tubulin polymerization upon presence of NPs was determined with biochemical assays (see the Supporting Information, Section XIV for the raw data). Data indicate that already NP concentrations below 1 nM significantly reduce polymerization of both actin and tubulin. Staining of vinculin indicated a reduction in focal adhesion contact areas A_{vinc}, see Fig. 13.6C. Additionally, atomic force microscopy (AFM) data showed that, in particular, for HUVECs the number N_{phyllo} and area A_{phyllo} of filopodia decreased upon exposure to NPs. Here again a difference between both cell types could be seen. Accompanying gene expression assays revealed the upregulation of several genes which are related to the cellular cytoskeleton, *cf.* Table 13.1. Taken together, the data demonstrate that NPs clearly have an impact on the cellular cytoskeleton, whereby

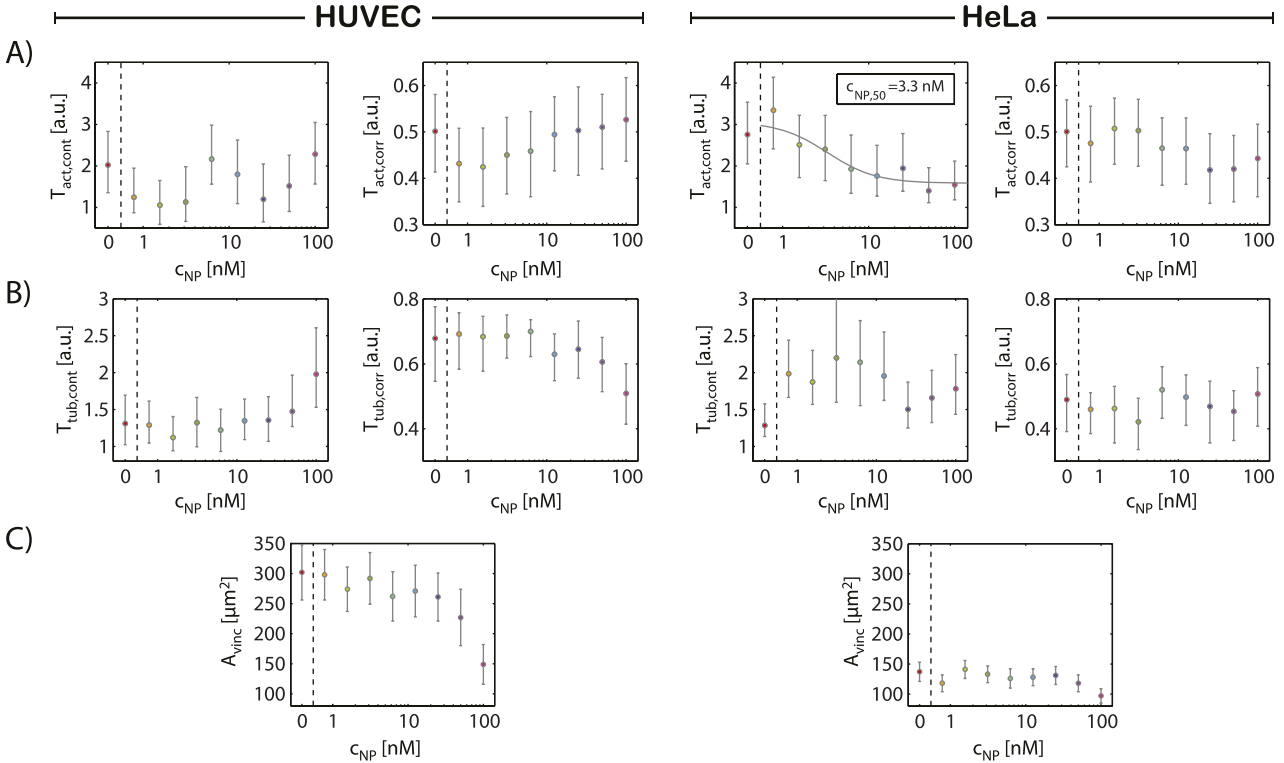

Figure 13.6 (A) Change of actin texture features (contrast $T_{act,cont}$, correlation $T_{act,corr}$) upon exposure of cells to Au-PMA* NPs. The results are presented as median ± lower/upper quartile for 600–1000 cells/condition. (B) Change of tubulin texture features (contrast $T_{tub,cont}$, correlation $T_{tub,corr}$) upon exposure of cells to Au-PMA* NPs. The results are presented as median ± lower/upper quartile for 60–150 cells/condition. (C) Focal adhesion area A_{vinc} after exposure of cells to Au-PMA* NPs. The results are presented as mean ± SD for 30 cells/condition.

detailed effects and in particular related NP doses vary between the investigated cell lines and conditions. In general, HUVECs seem to be more affected than HeLa cells (keeping in mind however the different levels of serum). Morphology changes occur at NP concentrations around $c_{NP,50} \approx 10$ nM, though this number can be seen only as an indicator for the order of magnitude. In contrast, it is safe to suggest that changes in gene expression are detected only at much higher NP concentrations than changes in morphology.

13.1.6 Deviation of Results Due to Aging of the Au-PMA NPs

Batch-to-batch variations were observed upon carrying out the assays used for assembling Table 13.1. In the Supporting Information therefore data obtained with different batches are indicated. However, also variation over time within the same batch was found. As general observation regarding cell viability, results obtained from the resazurin assay ("Marburg"), Au-PMA* NPs older than one year were found to be more toxic than the ones coated immediately before exposure of cells. In principle, the PMA shell around the NPs is stabilized by hydrophobic interaction, which leads to highly stable NPs. A detailed characterization in the direction has been provided by Huhn *et al.* [58]. On the other hand, after cellular incorporation, due to enzymatic degradation, part of the protecting PMA* shell may be lost over time [55], thus allowing for a closer contact of exposed cells to the Au surface. This demonstrates that NPs may change their toxicity over time.

This arises the question from where the toxicity originates, from the Au cores or form the PMA coating. We thus performed control measurements in which cells were exposed to empty PMA micelles, without Au cores inside the PMA shell (see the Supporting Information, Section IX.1 for the raw data). In agreement with previous studies [43], data confirmed that main toxicity arose from the Au cores and not from the PMA shell.

Table 13.2 Summary of the experimental results, in which cellular reaction to exposure to Au NPs with different surface chemistry was probed[a]

					Trend		$C_{NP,50}$ range [nM]	
	Feature	**Parameter**	**Variable**	**Derived from**	***HUVEC***	***HeLa***	***HUVEC***	***HeLa***
Au-PMA	*Viability*	Viability	V_{res}	Resazurin ("Marburg")	–	–	73–**82**–92	
		Proliferation rate	p	DNA synthesis	–	–	0.8–**1.0**–1.2	0.67–**1.3**–2.6
	Cell morphology	Area	A_{cell}	Actin (phalloidin)	–	0	50+	
			A_{nuclei}	DAPI	0	0		
	Lysosomes	Fraction of cell area	A_{lyso}/A_{cell}	LAMP1 (Ab) /actin (phalloidin)	++	++		
	Mitochondria	Zernike 0* order	Z^0_{mito}	Cell Light -mitochondria	+++	+++	0.13–**0.29**–0.64	0.080–**0.20**–0.51
Au-PEG	*Viability*	Viability	V_{res}	Resazurin ("Marburg")	–	0	2.6–**3.6**–5.1	
		Proliferation rate	p	DNA synthesis	–	o	35–**60**–100	
	Cell morphology	Area	A_{cell}	Actin (phalloidin)	–	0		
			A_{nuclei}	DAPI	0	0		

(*Continued*)

Table 13.2 (*Continued*)

	Feature	Parameter	Variable	Derived from	Trend		$C_{NP,50}$ range [nM]	
					HUVEC	***HeLa***	***HUVEC***	***HeLa***
	Lysosomes	Fraction of cell area	A_{lyso}/A_{cell}	LAMP1 (Ab) /actin (phalloidin)	++	0		
	Mitochondria	Zernike 0th order	Z^0_{mito}	CellLight -mitochondria	+	+	4.7–**7.4**–12	45–**46**-48
Au-MUA	*Viability*	Viability	V_{res}	Resazurin ("Marburg")	0	0		
		Proliferation rate	p	DNA synthesis	–	–	13–**19**–28	47–**80**–140
	Cell morphology	Area	A_{cell}	Actin (phalloidin)	–	0		
			A_{nuclei}	DAPI	0	0		
	Lysosomes	Fraction of cell area	A_{lyso}/A_{cell}	LAMP1 (Ab)/actin (phalloidin)	++	+		
	Mitochondria	Zernike 0* order	Z^0_{mito}	CellLight -mitochondria	0	0		
Au ions*	*Viability*	Viability	V_{res}	Resazurin ("Marburg")	–	0	64–**72**–81	
		Proliferation rate	p	DNA synthesis	–	–	10–**18**–34	36–**96**–250

	Feature	Parameter	Variable	Derived from	Trend		$C_{NP,50}$ range [nM]	
					HUVEC	***HeLa***	***HUVEC***	***HeLa***
	Cell morphology	Area	A_{cell}	Actin (phalloidin)	0	0		
			A_{nuclei}	DAPI	–	0	50+	
	Lysosomes	Fraction of cell area	A_{lyso}/A_{cell}	LAMP1 (Ab) /actin (phalloidin)	0	0		
	Mitochondria	Zernike 0^{th} order	Z^0_{mito}	CellLight -mitochondria	0/+	+	52–**55**–58	42–**51**–63
Cd ions*	*Viability*	Viability	V_{res}	Resazurin ("Marburg")	–	–	21–**24**–26	4.3–**13**-42
		Proliferation rate	p	DNA synthesis	–	–	3–**6**–13	0.37–**0.60**–0.96
	Cell morphology	Area	A_{cell}	Actin (phalloidin)	–	–	22–**28**–35	0.6–**2.3**–9.9
			A_{nuclei}	DAPI	–	–	50+	10+
	Lysosomes	Fraction of cell area	A_{lyso}/A_{cell}	LAMP1 (Ab)/actin (phalloidin)	o	o		
	Mitochondria	Zernike 0^{th} order	Z^0_{mito}	CellLight -mitochondria	0/+	++	27–**29**–30	1.8–**4.0**–8.9

[a]Reactions are shown in the trend column. c_NP_{50} describes the NP concentration at which half of the maximum effect was obtained. If a sigmoidal fit could be applied to the data, then the uncertainty is given in addition. The full data sets corresponding to this table are shown in the Supporting Information.

*For Au and Cd ions the indicated concentrations correspond to equivalent NP concentrations (see the Supporting Information for the corresponding calculation). Ab = antibody. Au-PMA NPs without fluorescence label were used.

13.1.7 Comparison of the Effects of Au-PMA NPs to the Effects of Au NPs with Different Surface Chemistry.

For comparison the effects on selected cellular parameters were investigated for Au NPs with different surface chemistry, *cf.* Table 13.2. Similarly to Au-PMA* NPs, strong effects on cellular viability in terms of proliferation and metabolic activity and the morphology of mitochondria were observed for Au-PMA NPs without a fluorescence label. In terms of cell viability, comparably strong impairments were only observed for Cd^{2+} ions at similar equivalent doses. MUA-coated NPs and Au salt seem to be less cytotoxic. In case of PEG NPs, HUVECs were more affected than HeLa cells regarding cytotoxicity, inhibited proliferation and changes in mitochondrial morphology. Data indicate that for example the effect of Au-PMA NPs on mitochondria seems to be specific, as in comparison to the other NPs, and in the Cd and Au salts a much stronger damage was observed. Also swelling of the lysosomes seems to be trigger more by NPs than by Cd and Au salts. In this way these observed changes in cell morphology are likely related to NP-induced toxicity, which can be different to the effects of other toxic agents. This may be related to the particular intracellular distribution of the NPs, which accumulate inside endosomes/lysosomes.

13.2 Conclusions

There are many published records in which cytotoxic effects of NPs on cells have been observed. Many of these reports focus on biochemical assays, probing cell viability or measuring gene expression levels. In this work we demonstrate that effects are also directly visible by changes in cellular morphology. Though there is an impressive amount of studies available in literature, quantitative comparison is hindered by the fact that on the one hand toxicity strongly depends on the type of NPs, and on the other hand the type of cells which have been used. In our study we performed many different assays with the same type of NP on two different types of cells, which allows for a quantitative comparison. In general, first effects upon exposure to NPs can be seen by a reduction in cellular proliferation rates. This

effect is already clearly visible at NP concentrations 1 or 2 orders of magnitude lower than the effects can be observed with standard cell viability assays. Also, changes in mitochondrial morphology can be measured which are an early indicator of NP-induced cellular damage. Then again lysosomal swelling and changes in cytoskeleton morphology occur at the same order of NP concentrations that cause significant reduction in cell viability. On the contrary, ROS production became prominent only at even higher concentrations.

The observed cellular changes induced by the Au NPs suggest a wide cascade of events that occur upon exposure of cultured cells to these engineered NPs. While previous results using these NPs have found that the Au-PMA NPs are not highly toxic and exert less toxicity than similarly sized and coated silver NPs, for instance [59], the extent of the effects observed here, even at low NP exposure concentrations, is quite surprising. The precise mechanism behind all these effects remains somewhat unclear and was outside of the scope of the current study.

The effect of the Au NPs on cell cytoskeleton, mitochondria, and lysosomes plays a major role in the possible functionality of the cells. As cell mitochondria are the main energy providers of the cells, any effect of the Au NPs on the mitochondria may affect the cellular energy reserves. As maintenance of lysosomal pH is an ATP-dependent process [60], the effect of the NPs on the lysosomal compartment may be associated with this loss in energy provision. Enlargement of the lysosomal compartment has been observed with different types of NPs, including quantum dots or iron oxide NPs, and has typically been associated with cellular adaptations in order to deal with the NP-induced stress [61, 62].

From a mechanistic point of view, changes in morphology due to exposure of high doses of NPs reduce the available “free” volume inside cells. The shape, polarity, and motility of cells are highly dependent on the normal morphology of organelles and subcellular structures, and organelles are interconnected by the cytoskeleton [63]. One of the important functions of the cytoskeleton is to dynamically arrange organelles at certain places inside the cells. If the accumulation of Au NPs affects the cytoskeletons, then the attached organelles will be affected too. Our data show that the structure of cytoskeleton was affected dramatically as the intracellular Au NP concentration increased. Consequently, the

sizes of the cells treated with high doses of Au NPs were much smaller than the control group, and the organelles were all crowded around the nucleus. Also, the endocytosis of NPs caused swelling of lysosomes, and the intracellular area occupied by lysosomes increased consequently. Also this may interfere with the location and distribution of other organelles and subcellular structures in the cell. The enlarged cellular lysosomal compartment may sterically hinder the cellular cytoskeletal architecture, forcing the cells to remodel their cytoskeleton [62]. In recent work, it has also been shown that NP-mediated cellular energy losses can affect cellular signaling pathways that directly influence cell cytoskeleton, such as induction of autophagy or activation of small GTPases [64, 65].

Various intracellular signaling pathways are associated with the proper functioning of the cellular cytoskeleton [66]. Any alterations in cytoskeleton architecture can therefore have profound effects on various cellular functions such as cellular motility [67]. and result in a decrease in cell proliferation, as observed here and in other reports [62]. A key mediator in cytoskeleton-associated signaling is the FAC, which connects the actin cytoskeleton to the extracellular matrix *via* transmembrane integrins [68]. In line with our expectations, a clear concentration-dependent loss in FACs was observed, which is most outspoken for the HUVEC cells. The effects on cell functionality affected cellular signaling were also assessed via gene expression assays that revealed the upregulation of several genes which are related to the cellular cytoskeleton, *cf.* Table 13.1. Of the genes that show significant upregulation, mainly *mapk13* and *mapt* show the highest level of difference between HUVEC and HeLa cells. *Mapk13* encodes a member of the mitogen-activated protein (MAP) kinase family that acts as an integration point for multiple biochemical signals and is involved in a wide variety of cellular processes such as proliferation, differentiation, transcription regulation, and development. The MAP kinase is known to be activated by cellular stress. *Mapt* encodes for microtubule-associated protein Tau, which is known to be a key player in the onset of Alzheimer's disease. In terms of cytoskeleton functionality, Tau can sterically stabilize microtubules in an attempt to prevent loss of function [69]. Taken together, these data suggest a clear indication of cellular stress elicited by the Au NPs that results in mitochondrial damage and

affects cytoskeleton-associated signaling at concentrations far lower than those at which clear cytotoxicity is typically observed.

Possible mechanisms behind these findings could lie in the inert nature of the Au NPs, which, when incorporated into the cellular endosomal compartment, may affect the overall cellular degradative capacity. While instability of the lysosomal membrane may induce necrosis [70], this did not appear to be the case here, as no typical markers for necrosis were found under NP concentrations where lysosomes were affected. The presence of the Au NPs may however impose an alkalizing effect on the lysosomes and can therefore result in a partial loss of function of the endolysosomal compartment [20]. In response, the cell will try to compensate for this loss of degradative function, which can result in the synthesis of additional lysosomes and/or induction of autophagy [61]. These additional lysosomes or the occurrence of autophagosomes may directly affect cell cytoskeleton architecture, either through steric hindrance and remodeling [62] or through activation of cellular signaling pathways involved in both autophagy and actin cytoskeleton modeling [71]. Additionally, these processes require energy in the form of ATP and will therefore impose stress on the cellular mitochondria. As Au NPs are well-known to cause oxidative stress, the additional activation of mitochondrial oxidative phosphorylation pathways, a major source of cellular ATP as well as oxidative stress, may further stress the mitochondria. These data are also in line with a recent study displaying that rapid cellular internalization of rigid NPs through energy-dependent processes also stresses cellular mitochondria by overactivating ATP production, coupled with the intrinsic oxidative stress caused by the NPs [65]. Together, these data link the observed effects to two main mechanisms, being the loss of degradative capacity of the cells along with cellular adaptation to the presence of these NPs and their associated ROS and energy demands.

Our data suggest that not all indicators for NP toxicity have the same sensitivity. Cellular proliferation and alterations in mitochondrial morphology are clearly early indicators. Prior to when changes in cellular viability are observable, there are already detectable changes in (sub-) cellular morphology. Geometrical changes in certain cellular compartments occur already at surprisingly low NP concentrations, in particular in mitochondria. Most likely these effects can be linked to the surface chemistry of

the used Au NPs as the observed changes vary among the different surface coatings which were being tested.

In this way, just by visual inspection of cells (upon appropriate immunostaining) NP-related toxicity can be observed *via* morphological analysis. In our case of polymer-coated Au NPs, even at NP concentrations where no significant oxidative stress (ROS production) can be detected, morphology can already be altered significantly. These morphological changes provide a reliable assessment for the effect of NPs on the cellular homeostasis. Therefore, the determination of toxic effects of NP exposure based on morphological features may be an attractive alternative methodology for situations in which fixed samples, such as tissue sample from a biopsy, have to be inspected, and in which case the use of biochemical assays can no longer be applied. Morphology changes seem to be in particular in the case of mitochondria and lysosomes related to NP-induced toxicity and are different to changes observed upon exposure of cells to toxic metal salts.

13.3 Materials and Methods

Polymer-coated Au NPs (Au-PMA* NPs) [12, 35–37] with a core diameter of $d_c = 4.8 \pm 0.7$ nm (as determined by transmission electron microscopy (TEM)), a hydrodynamic diameter of $d_h = 12 \pm 3$ nm (as determined from the number distribution of dynamic light scattering (DLS) in water), and a zeta-potential of $\zeta = -30 \pm 2$ nm (as determined from laser Doppler anemometry (LDA) in water) were used. Due to a fluorophore which is located inside the inner hydrophobic polymer shell, and thus in first order not present at the NP surface, these NPs are fluorescent and thus can be visualized with confocal microscopy. Also the control NPs, i.e., Au-PMA NPs (without fluorescence label in the polymer shell), Au-MUA NPs [47], and Au-PEG NPs [44, 47, 73], were synthesized according to previously published protocols. The full protocol of synthesis and characterization of the NPs are located in the Supporting Information, Sections I and II. HUVECs and HeLa cells were exposed to the NPs at concentrations ranging from 0.1–100 nM in serum containing medium (Supporting Information, Section III). In parallel, Au^{3+} and Cd^{2+} ions were added at the same amount of total Au atoms for the Au NPs (0–35 mM).

Their uptake was quantified by confocal microscopy and standard viability and proliferation assays (Live/Dead viability assay [74], cell proliferation assay [75], resazurin assay [76–78], and MTT assay [79]). Different cellular structures (lysosomes, mitochondria, actin and microtubule network, vinculin, and filopodia) were optionally labeled by immunostaining or transfection, and changes in their geometry as well as changes in the morphology of the whole cell (i.e., cell spreading) were analyzed from fluorescence or atomic force microscopy (AFM) images by digital image analysis tools. In addition, the effects of the NPs on expression of genes related to the cytoskeleton as well as actin and tubulin polymerization assays were carried out [80, 81].

Supporting Information

The Supporting Information is available free of charge on the ACS Publications website at DOI: 10.1021/acsnano.7b01760.

Detailed protocols and raw data (PDF): http://pubs.acs.org/doi/suppl/10.1021/acsnano.7b01760/suppl_file/nn7b01760_si_001.pdf

Author Contributions

X.M. was responsible for cell culture and involved in CLSM and TEM imaging. R.H. performed parts of the microscopic imaging and the major part of the image processing, data analysis, and assembly of figures and graphs. D.J.deA., D.V., and B.P. prepared and characterized the nanoparticles. D.V. conducted the actin/tubulin polymerization and cytotoxicity assays. S.J.S. and B.M. performed several cyto-/genotoxocity assays. F.Y., J.F., and C.R. did AFM imaging, while H.V. and N.F. performed HIM imaging. N.F. carried out the flow cytometer experiments. M.S. and R.T. did the in vivo zebrafish experiments. N.H., A.G., X.-J.L., and W.J.P. designed the experiments. R.H. and W.J.P. wrote the major part of the manuscript.

Notes

The authors declare no competing financial interest.

Acknowledgments

This work was supported by the Deutsche Forschungsgemeinschaft (project PA 794/25-1 to W.J.P.) and the Chinesisch-Deutsches Zentrum fur Wissenschaftsforderung (project GZ905 to W.J.P.). N.F. acknowledges funding from the Swedish Governmental Agency for Innovation Systems (Vinnova).

References

1. Auffan, M.; Rose, J.; Bottero, J.-Y.; Lowry, G. V.; Jolivet, J.-P.; Wiesner, M. R. Towards a Definition of Inorganic Nanoparticles from an Environmental, Health and Safety Perspective. *Nat. Nanotechnol.* **2009,** 4, 634–641.
2. Alkilany, A.; Murphy, C. Toxicity and Cellular Uptake of Gold Nanoparticles: What We Have Learned So Far? *J. Nanopart. Res.* **2010,** 12, 2313–2333.
3. Canton, I.; Battaglia, G. Endocytosis at the Nanoscale. *Chem. Soc. Rev.* **2012,** 41, 2718–2739.
4. Nazarenus, M.; Zhang, Q.; Soliman, M. G.; del Pino, P.; Pelaz, B.; Carregal-Romero, S.; Rejman, J.; Rothen-Ruthishauser, B.; Clift, M. J. D.; Zellner, R.; Nienhaus, G. U.; Delehanty, J. B.; Medintz, I. L.; Parak, W. J. In Vitro Interaction of Colloidal Nanoparticles with Mammalian Cells: What Have We Learned Thus Far? *Beilstein J. Nanotechnol.* **2014,** 5, 1477–1490.
5. Bertoli, F.; Davies, G. L.; Monopoli, M. P.; Moloney, M.; Gun'ko, Y. K.; Salvati, A.; Dawson, K. A. Magnetic Nanoparticles to Recover Cellular Organelles and Study the Time Resolved Nanoparticle-Cell Interactome throughout Uptake. *Small* **2014,** 10, 3307–3315.
6. Lesniak, A.; Fenaroli, F.; Monopoli, M. R.; Aberg, C.; Dawson, K. A.; Salvati, A. Effects of the Presence or Absence of a Protein Corona on Silica Nanoparticle Uptake and Impact on Cells. *ACS Nano* **2012,** 6, 5845–5857.
7. Perez-Hernandez, M.; Del Pino, P.; Mitchell, S. G.; Moros, M.; Stepien, G.; Pelaz, B.; Parak, W. J.; Galvez, E. M.; Pardo, J.; de la Fuente, J. M. Dissecting the Molecular Mechanism of Apoptosis during Photothermal Therapy Using Gold Nanoprisms. *ACS Nano* **2015,** 9,52–61.
8. Nel, A. E.; Madler, L.; Velegol, D.; Xia, T.; Hoek, E. M. V.; Somasundaran, P.; Klaessig, F.; Castranova, V.; Thompson, M. Understanding

Biophysicochemical Interactions at the Nano-Bio Interface. *Nat. Mater.* **2009,** 8, 543–557.

9. Xia, T.; Rome, L.; Nel, A. Nanobiology - Particles Slip Cell Security. *Nat. Mater.* **2008,** 7, 519–520.
10. Setyawati, M. I.; Khoo, P. K. S.; Eng, B. H.; Xiong S.; Zhao, X.; Das, G. K.; Tan, T. T.-Y.; Loo, J. S. C.; Leong, D. T.; Ng, K. W. Cytotoxic and Genotoxic Characterization of Titanium Dioxide, Gadolinium Oxide, and Poly(lactic-co-glycolic acid) Nanoparticles in Human Fibroblasts. *J. Biomed. Mater. Res., Part A* **2013,** *101A,* 633–640.
11. Anguissola, S.; Garry, D.; Salvati, A.; O'Brien, P. J.; Dawson, K A. High Content Analysis Provides Mechanistic Insights on the Pathways of Toxicity Induced by Amine-Modified Polystyrene Nanoparticles. *PLoS One* **2014,** *9,* e108025.
12. Soenen, S. J.; Manshian, B.; Montenegro, J. M.; Amin, F.; Meermann, B.; Thiron, T.; Cornelissen, M.; Vanhaecke, F.; Doak, S.; Parak, W. J.; De Smedt, S.; Braeckmans, K. Cytotoxic Effects of Gold Nanoparticles: A Multiparametric Study. *ACS Nano* **2012,** *6,* 5767–5783.
13. Jan, E.; Byrne, S. J.; Cuddihy, M.; Davies, A. M.; Volkov, Y.; Gun'ko, Y. K.; Kotov, N. A. High-Content Screening as a Universal Tool for Fingerprinting of Cytotoxicity of Nanoparticles. *ACS Nano* **2008,** *2,* 928 938.
14. Wang, F.; Bexiga, M. G.; Anguissola, S.; Boya, P.; Simpson, J. C.; Salvati, A.; Dawson, K. A. Time Resolved Study of Cell Death Mechanisms Induced by Amine-Modified Polystyrene Nanoparticles. *Nanoscale* **2013,** *5,* 10868 10876.
15. Pan, Y.; Leifert, A.; Ruau, D.; Neuss, S.; Bornemann, J.; Schmid, G.; Brandau, W.; Simon, U.; Jahnen-Dechent, W. Gold Nanoparticles of Diameter 1.4 nm Trigger Necrosis by Oxidative Stress and Mitochondrial Damage. *Small* **2009,** *5,* 2067 2076.
16. Chompoosor, A.; Saha, K.; Ghosh, P. S.; Macarthy, D. J.; Miranda, O. R.; Zhu, Z. J.; Arcaro, K. F.; Rotello, V. M. The Role of Surface Functionality on Acute Cytotoxicity, ROS Generation and DNA Damage by Cationic Gold Nanoparticles. *Small* **2010,** *6,* 2246–2249.
17. Mkandawire, M. M.; Lakatos, M.; Springer, A.; Clemens, A.; Appelhans, D.; Krause-Buchholz, U.; Pompe, W.; Rodel, G.; Mkandawire, M. Induction of Apoptosis in Human Cancer Cells by Targeting Mitochondria with Gold Nanoparticles. *Nanoscale* **2015,** *7,* 10634–10640.
18. Wang, L.; Liu, Y.; Li, W.; Jiang, X.; Ji, Y.; Wu, X.; Xu, L.; Qiu, Y.; Zhao, K.; Wei, T.; Li, Y.; Zhao, Y.; Chen, C. Selective Targeting of Gold Nanorods at the

Mitochondria of Cancer Cells: Implications for Cancer Therapy. *Nano Lett.* **2011,** 11, 772–780.

19. Bexiga, M. G.; Kelly, C.; Dawson, K. A.; Simpson, J. C. RNAi-Mediated Inhibition of Apoptosis Fails to Prevent Cationic Nano-particle-Induced Cell Death in Cultured Cells. *Nanomedicine* (*London, U. K.*) **2014,** *9,* 1651–1664.
20. Ma, X.; Wu, Y.; Jin, S.; Tian, Y.; Zhang, X.; Zhao, Y.; Yu, L.; Liang, X.-J. Gold Nanoparticles Induce Autophagosome Accumulation through Size-Dependent Nanoparticle Uptake and Lysosome Impairment. *ACS Nano* **2011,** 5, 8629–8639.
21. Mahmoudi, M.; Abdelmonem, A. M.; Behzadi, S.; Clement, J. H.; Dutz, S.; Ejtehadi, M. R.; Hartmann, R.; Kantner, K.; Linne, U.; Maffre, P.; Metzler, S.; Moghadam, M. K.; Pfeiffer, C.; Rezaei, M.; Ruiz-Lozano, P.; Serpooshan, V.; Shokrgozar, M. A.; Nienhaus, G. U.; Parak, W. J. Temperature: The "Ignored" Factor at the NanoBio Interface. *ACS Nano* **2013,** 7, 6555–6562.
22. Ott, A.; Yu, X.; Hartmann, R.; Rejman, J.; Schutz, A.; Ochs, M.; Parak, W. J.; Carregal-Romero, S. Light-Addressable and Degradable Silica Capsules for Delivery of Molecular Cargo to the Cytosol of Cells. *Chem. Mater.* **2015,** 27, 1929–1942.
23. Gunduz, N.; Ceylan, H.; Guler, M. O.; Tekinay, A. B. Intracellular Accumulation of Gold Nanoparticles Leads to Inhibition of Macropinocytosis to Reduce the Endoplasmic Reticulum Stress. *Sci. Rep.* **2017,** 7, 40493.
24. Gonnissen, D.; Qu, Y.; Langer, K.; Ozturk, C.; Zhao, Y.; Chen, C.; Seebohm, G.; Dufer, M.; Fuchs, H.; Galla, H. J.; Riehemann, K. Comparison of Cellular Effects of Starch-Coated SPIONs and Poly(lactic-co-glycolic acid) Matrix Nanoparticles on Human Mono-cytes. *Int. J. Nanomed.* **2016,** 11, 5221–5236.
25. Pernodet, N.; Fang, X. H.; Sun, Y.; Bakhtina, A.; Ramakrishnan, A.; Sokolov, J.; Ulman, A.; Rafailovich, M. Adverse Effects of Citrate/Gold Nanoparticles on Human Dermal Fibroblasts. *Small* **2006,** *2,* 766 773.
26. Wu, Y.-L.; Putcha, N.; Ng, K. W.; Leong, D. T.; Lim, C. T.; Loo, S. C. J.; Chen, X. Biophysical Responses upon the Interaction of Nanomaterials with Cellular Interfaces. *Acc. Chem. Res.* **2013,** *46,* 782–791.
27. Allen, L. T.; Fox, E. J. P.; Blute, I.; Kelly, Z. D.; Rochev, Y.; Keenan, A. K.; Dawson, K. A.; Gallagher, W. M. Interaction of Soft Condensed Materials With Living Cells: Phenotype/Transcriptome Correlations for the Hydrophobic Effect. *Proc. Natl. Acad. Sci. U. S. A.* **2003,** *100,* 6331–6336.

28. Mironava, T.; Hadjiargyrou, M.; Simon, M.; Jurukovski, V.; Rafailovich, M. H. Gold Nanoparticles Cellular Toxicity and Recovery: Effect of Size, Concentration and Exposure Time. *Nanotoxicology* **2010,** *4,* 120–137.

29. Yang, J. A.; Lohse, S. E.; Murphy, C. J. Tuning Cellular Response to Nanoparticles *via* Surface Chemistry and Aggregation. *Small* **2014,** 10, 1642–1651.

30. Setyawati, M. I.; Tay, C. Y.; Chia, S. L.; Goh, S. L.; Fang, W.; Neo, M. J.; Chong, H. C.; Tan, S. M.; Loo, S. C. J.; Ng, K. W.; Xie, J. P.; Ong, C. N.; Tan, N. S.; Leong, D. T. Titanium Dioxide Nanomaterials Cause Endothelial Cell Leakiness by Disrupting the Homophilic Interaction of VE-cadherin. *Nat. Commun.* **2013,** *4,* 1673.

31. Qiu, Y.; Tong, S.; Zhang, L.; Sakurai, Y.; Myers, D. R.; Hong, L.; Lam, W. A.; Bao, G. Magnetic Forces Enable Controlled Drug Delivery by Disrupting Endothelial Cell-Cell Junctions. *Nat. Commun.* **2017,** 8, 15594.

32. Lin, I. C.; Liang, M.; Liu, T.-Y.; Ziora, Z. M.; Monteiro, M. J.; Toth, I. Interaction of Densely Polymer-Coated Gold Nanoparticles with Epithelial Caco-2 Monolayers. *Biomacromolecules* **2011** , *12,* 1339–1348.

33. Ng, C. T.; Yung, L. Y. L.; Swa, H. L. F.; Poh, R. W. Y.; Gunaratne, J.; Bay, B. H. Altered Protein Expression Profile Associated with Phenotypic Changes in Lung Fibroblasts Co-Cultured with Gold Nanoparticle-Treated Small Airway Epithelial Cells. *Biomaterials* **2015,** *39*,31–38.

34. Mironava, T.; Hadjiargyrou, M.; Simon, M.; Rafailovich, M. H. Gold Nanoparticles Cellular Toxicity and Recovery: Adipose Derived Stromal Cells. *Nanotoxicology* **2014,** 8, 189–201.

35. Pellegrino, T.; Manna, L.; Kudera, S.; Liedl, T.; Koktysh, D.; Rogach, A. L.; Keller, S.; Radler, J.; Natile, G.; Parak, W. J. Hydrophobic Nanocrystals Coated with an Amphiphilic Polymer Shell: A General Route to Water Soluble Nanocrystals. *Nano Lett.* **2004,** *4,* 703–707.

36. Lin, C.-A. J.; Sperling, R. A.; Li, J. K.; Yang, T.-Y.; Li, P.-Y.; Zanella, M.; Chang, W. H.; Parak, W. J. Design of an Amphiphilic Polymer for Nanoparticle Coating and Functionalization. *Small* **2008,** *4,* 334–341.

37. Zhang, F.; Lees, E.; Amin, F.; Rivera_Gil, P.; Yang, F.; Mulvaney, P.; Parak, W. J. Polymer-Coated Nanoparticles: A Universal Tool for Biolabelling Experiments. *Small* **2011** , *7,* 3113–3127.

38. Charron, G.; Huhn, D.; Perrier, A.; Cordier, L.; Pickett, C. J.; Nann, T.; Parak, W. J. On the Use of pH Titration to Quantitatively Characterize Colloidal Nanoparticles. *Langmuir* **2012,** *28,* 15141–15149.

39. Huhn, D.; Kantner, K.; Geidel, C.; Brandholt, S.; De Cock, I.; Soenen, S. J. H.; Rivera_Gil, P.; Montenegro, J.-M.; Braeckmans, K.; Mullen, K.; Nienhaus, G. U.; Klapper, M.; Parak, W. J. Polymer-Coated Nanoparticles Interacting with Proteins and Cells: Focusing on the Sign of the Net Charge. *ACS Nano* **2013,** *7,* 3253–3263.

40. Harakeh, S.; Abdel-Massih, R. M.; Rivera_Gil, P.; Sperling, R. A.; Meinhardt, A.; Niedwiecki, A.; Rath, M.; Parak, W. J.; Baydoun, E. The Effect of PEG-Coated Gold Nanoparticles on the Anti-proliferative Potential of Specific Nutrient Synergy. *Nanotoxicology* **2010,** *4,* 177–185.

41. Rothen-Rutishauser, B.; Kuhn, D. A.; Ali, Z.; Gasser, M.; Amin, F.; Parak, W. J.; Vanhecke, D.; Fink, A.; Gehr, P.; Brandenberger, C. Quantification of Gold Nanoparticle Cell Uptake under Controlled Biological Conditions and Adequate Resolution. *Nanomedicine* (*London, U. K.*) **2014,** 9, 607–621.

42. Schweiger, C.; Hartmann, R.; Zhang, F.; Parak, W. J.; Kissel, T.; Rivera_Gil, P. Quantification of the Internalization Patterns of Superparamagnetic Iron Oxide Nanoparticles with Opposite Charge. *J. Nanobiotechnol.* **2012,** 10, 28.

43. Lehmann, A. D.; Parak, W. J.; Zhang, F.; Ali, Z.; Rocker, C.; Nienhaus, G. U.; Gehr, P.; Rothen-Rutishauser, B. Fluorescent-Magnetic Hybrid Nanoparticles Induce a Dose-Dependent Increase in Proinflammatory Response in Lung Cells in Vitro Correlated with Intracellular Localization. *Small* **2010,** *6,* 753–762.

44. Soenen, S. J.; Manshian, B. B.; Abdelmonem, A. M.; Montenegro, J.-M.; Tan, S.; Balcaen, L.; Vanhaecke, F.; Brisson, A. R.; Parak, W. J.; De Smedt, S. C.; Braeckmans, K. The Cellular Interactions of PEGylated Gold Nanoparticles: Effect of PEGylation on Cellular Uptake and Cytotoxicity. *Part. Part. Syst. Charact.* **2014,** *31,* 794–800.

45. Pan, Y.; Neuss, S.; Leifert, A.; Fischler, M.; Wen, F.; Simon, U.; Schmid, G.; Brandau, W.; Jahnen-Dechent, W. Size-Dependent Cytotoxicity of Gold Nanoparticles. *Small* **2007,** 3, 1941–1949.

46. Shukla, R.; Bansal, V.; Chaudhary, M.; Basu, A.; Bhonde, R. R.; Sastry, M. Biocompatibility of Gold Nanoparticles and Their Endocytotic Fate Inside the Cellular Compartment: A Microscopic Overview. *Langmuir* **2005,** 21, 10644–10654.

47. Caballero-Dfaz, E.; Pfeiffer, C.; Kastl, L.; Rivera-Gil, P.; Simonet, B.; Valcarcel, M.; Jimenez-Lamana, J.; Laborda, F.; Parak, W. J. The Toxicity of Silver Nanoparticles Depends on Their Uptake by Cells and Thus

on Their Surface Chemistry. *Part. Part. Syst. Charact.* **2013,** *30,* 1079–1085.

48. del_Pino, P.; Yang, F.; Pelaz, B.; Zhang, Q.; Kantner, K.; Hartmann, R.; Baroja, N. M. d.; Gallego, M.; Moller, M.; Manshian, B. B.; Soenen, S. J.; Riedel, R.; Hampp, N.; Parak, W. J. Basic Physicochemical Properties of Polyethylene Glycol Coated Gold Nanoparticles that Determine Their Interaction with Cells. *Angew. Chem., Int. Ed.* **2016,** 55, 5483–5487.
49. Kirchner, C.; T, L.; Kudera, S.; Pellegrino, T.; Munoz Javier, A.; Gaub, H. E.; Stolzle, S.; Fertig, N.; Parak, W. J. Cytotoxicity of Colloidal CdSe and CdSe/ZnS Nanoparticles. *Nano Lett.* **2005,** *5,* 331–338.
50. Chithrani, B. D.; Chan, W. C. W. Elucidating the Mechanism of Cellular Uptake and Removal of Protein-Coated Gold Nanoparticles of Different Sizes and Shapes. *Nano Lett.* **2007,** 7, 1542–1550.
51. Chithrani, B. D.; Ghazani, A. A.; Chan, W. C. W. Determining the Size and Shape Dependence of Gold Nanoparticle Uptake into Mammalian Cells. *Nano Lett.* **2006,** *6,* 662 668.
52. Sultani, A. B.; Marquez-Curtis, L. A.; Elliott, J. A. W.; McGann, L. E. Improved Cryopreservation of Human Umbilical Vein Endothelial Cells: A Systematic Approach. *Sci. Rep.* **2016,** *6,* 34393.
53. Soenen, S. J. H.; De Meyer, S. F.; Dresselaers, T.; Velde, G. V.; Pareyn, I. M.; Braeckmans, K.; De Cuyper, M.; Himmelreich, U.; Vanhoorelbeke, K. I. MRI Assessment of Blood Outgrowth Endothelial Cell Homing Using Cationic Magnetoliposomes. *Biomaterials* **2011,** 32, 4140–4150.
54. Su, G. X.; Zhou, X. F.; Zhou, H. Y.; Li, Y.; Zhang, X. R.; Liu, Y.; Cao, D. P.; Yan, B. Size-Dependent Facilitation of Cancer Cell Targeting by Proteins Adsorbed on Nanoparticles. *ACS Appl. Mater. Interfaces* **2016,** *8,* 30037–30047.
55. Kreyling, W. G.; Abdelmonem, A. M.; Ali, Z.; Alves, F.; Geiser, M.; Haberl, N.; Hartmann, R.; Hirn, S.; de Aberasturi, D. J.; Kantner, K.; Khadem-Saba, G.; Montenegro, J. M.; Rejman, J.; Rojo, T.; de Larramendi, I. R.; Ufartes, R.; Wenk, A.; Parak, W. J. In Vivo Integrity of Polymer-Coated Gold Nanoparticles. *Nat. Nanotechnol.* **2015,** *10,* 619–623.
56. Boland, M. V.; Markey, M. K.; Murphy, R. F. Automated Recognition of Patterns Characteristic of Subcellular Structures in Fluorescence Microscopy Images. *Cytometry* **1998,** *33,* 366–375.
57. Haralick, R. M. Statistical and Structural Approaches to Texture. *Proc. IEEE* **1979,** *67,* 786 804.
58. Huhn, J.; Carrillo-Carrion, C.; Soliman, M. G.; Pfeiffer, C.; Valdeperez, D.; Masood, A.; Chakraborty, I.; Zhu, L.; Gallego, M.; Zhao, Y.; Carril, M.;

Feliu, N.; Escudero, A.; Alkilany, A. M.; Pelaz, B.; del Pino, P.; Parak, W. J. Selected Standard Protocols for the Synthesis, Phase Transfer, and Characterization of Inorganic Colloidal Nanoparticles. *Chem. Mater.* **2017,** *29,* 399–461.

59. Manshian, B. B.; Pfeiffer, C.; Pelaz, B.; Heimerl, T.; Gallego, M.; Moller, M.; del Pino, P.; Himmelreich, U.; Parak, W. J.; Soenen, S. J. High-Content Imaging and Gene Expression Approaches To Unravel the Effect of Surface Functionality on Cellular Interactions of Silver Nanoparticles. *ACS Nano* **2015,** 9, 10431 – 10444.
60. Ramfrez-Peinado, S.; Leon-Annicchiarico, C. L.; Galindo-Moreno, J.; Iurlaro, R.; Caro-Maldonado, A.; Prehn, J. H. M.; Ryan, K. M.; Munoz-Pinedo, C. Glucose-Starved Cells Do Not Engage in Prosurvival Autophagy. *J. Biol. Chem.* **2013,** 288, 30387–30398.
61. Neibert, K. D.; Maysinger, D. Mechanisms of Cellular Adaptation to Quantum Dots-the Role of Glutathione and Transcription Factor EB. *Nanotoxicology* **2012,** *6,* 249 262.
62. Soenen, S. J. H.; Nuytten, N.; De Meyer, S. F.; De Smedt, S. C.; De Cuyper, M. High Intracellular Iron Oxide Nanoparticle Concentrations Affect Cellular Cytoskeleton and Focal Adhesion Kinase-Mediated Signaling. *Small* **2010,** 6, 832–842.
63. Rafelski, S. M.; Marshall, W. F. Building the Cell: Design Principles of Cellular Architecture. *Nat. Rev. Mol. Cell Biol.* **2008,** *9,* 593 602.
64. Manshian, B. B.; Pokhrel, S.; Madler, L.; Himmelreich, U.; Soenen, S. J. The Impact of Nanoparticle-Driven Lysosomal Alkalinization on Cellular Functionality. *submitted.*
65. Manshian, B. B.; Himmelreich, U.; Soenen, S. J. Standard Cellular Testing Conditions Generate an Exaggerated Nanoparticle Cytotoxicity Profile. *Chem. Res. Toxicol.* **2017,** *30,* 595 603.
66. Schappi, J. M.; Krbanjevic, A.; Rasenick, M. M. Tubulin, Actin and Heterotrimeric G Proteins: Coordination of Signaling and Structure. *Biochim. Biophys. Acta, Biomembr.* **2014,** *1838,* 674–681.
67. Tay, C. Y.; Cai, P.; Setyawati, M. I.; Fang, W.; Tan, L. P.; Hong, C. H.; Chen, X.; Leong, D. T. Nanoparticles Strengthen Intracellular Tension and Retard Cellular Migration. *Nano Lett.* **2014,** *14*,83–88.
68. Hall, J. E.; Fu, W.; Schaller, M. D. Focal Adhesion Kinase: Exploring Fak Structure to Gain Insight into Function. *Int. Rev. Cell Mol. Biol.* **2011,** 288, 185–225.
69. Chung, P. J.; Choi, M. C.; Miller, H. P.; Feinstein, H. E.; Raviv, U.; Li, Y.; Wilson, L.; Feinstein, S. C.; Safinya, C. R. Direct Force Measurements Reveal That Protein Tau Confers Short-Range Attractions and Isoform

Dependent Steric Stabilization to Micro-tubules. *Proc. Natl. Acad. Sci. U. S. A.* **2015,** 112, E6416–E6425.

70. Lai, L.; Jin, J. C.; Xu, Z. Q.; Mei, P.; Jiang, F. L.; Liu, Y. Necrotic Cell Death Induced by the Protein-Mediated Intercellular Uptake of CdTe Quantum Dots. *Chemosphere* **2015,** *135,* 240–249.
71. Monastyrska, I.; Rieter, E.; Klionsky, D. J.; Reggiori, F. Multiple Roles of the Cytoskeleton in Autophagy. *Biol. Rev.* **2009,** 84, 431–448.
72. Amin, F.; Yushchenko, D. A.; Montenegro, J. M.; Parak, W. J. Integration of Organic Fluorophores in the Surface of Polymer-Coated Colloidal Nanoparticles for Sensing the Local Polarity of the Environment. *ChemPhysChem* **2012,** 13, 1030–1035.
73. Sperling, R. A.; Pellegrino, T.; Li, J. K.; Chang, W. H.; Parak, W. J. Electrophoretic Separation of Nanoparticles with a Discrete Number of Functional Groups. *Adv. Funct. Mater.* **2006,** 16, 943–948.
74. Papadopoulos, N. G.; Dedoussis, G. V. Z.; Spanakos, G.; Gritzapis, A. D.; Baxevanis, C. N.; Papamichail, M. An Improved Fluorescence Assay for the Determination of Lymphocyte-Mediated Cytotoxicity Using Flow Cytometry. *J. Immunol. Methods* **1994,** 177, 101 – 111.
75. Salic, A.; Mitchison, T. J. A Chemical Method for Fast and Sensitive Detection of DNA Synthesis in Vivo. *Proc. Natl. Acad. Sci. U. S. A.* **2008,** 105, 2415–2420.
76. O'Brien, J.; Wilson, I.; Orton, T.; Pognan, F. o. Investigation of the Alamar Blue (Resazurin) Fluorescent Dye for the Assessment of Mammalian Cell Cytotoxicity. *Eur. J. Biochem.* **2000,** 267, 5421–5426.
77. Van Hoecke, K.; De Schamphelaer, K. A. C.; Ali, Z.; Zhang, F.; Elsaesser, A.; Rivera_Gil, P.; Parak, W. J.; Smagghe, G.; Janssen, C. R. Ecotoxicity and Uptake of Polymer Coated Gold Nanoparticles. *Nanotoxicology* **2013,** 7,37–47.
78. Singh, M. P.; Atkins, T. M.; Muthuswamy, E.; Kamali, S.; Tu, C.; Louie, A. Y.; Kauzlarich, S. M. Development of Iron-Doped Silicon Nanoparticles As Bimodal Imaging Agents. *ACS Nano* **2012,** *6,* 5596–5604.
79. Magrez, A.; Horvath, L.; Smajda, R.; Salicio, V.; Pasquier, N.; Forro, L.; Schwaller, B. Cellular Toxicity of TiO2-Based Nanofilaments. *ACS Nano* **2009,** *3,* 2274–2280.
80. Kouyama, T.; Mihashi, K. Fluorimetry Study of N-(1-Pyrenyl) iodoacetamide-Labelled F-Actin. *Eur. J. Biochem.* **1981,** 114, 33–38.
81. Bonne, D.; Heusele, C.; Simon, C.; Pantaloni, D. 4',6- Diamidino-2-Phenylindole, a Fluorescent Probe for Tubulin and Microtubules. *J. Biol. Chem.* **1985,** 260, 2819–2825.